

Effect of Sample Heterogeneity on the Interpretation of Quartz Crystal Microbalance Data: Impurity Effects

Elena Rojas, Marta Gallego, and Ilya Reviakine

Anal. Chem., **2008**, 80 (23), 8982-8990 • DOI: 10.1021/ac8012829 • Publication Date (Web): 27 October 2008

Downloaded from <http://pubs.acs.org> on March 21, 2009

More About This Article

Additional resources and features associated with this article are available within the HTML version:

- Supporting Information
- Access to high resolution figures
- Links to articles and content related to this article
- Copyright permission to reproduce figures and/or text from this article

[View the Full Text HTML](#)



Effect of Sample Heterogeneity on the Interpretation of Quartz Crystal Microbalance Data: Impurity Effects

Elena Rojas, Marta Gallego, and Ilya Reviakine*

Centro de Investigación Cooperativa en Biomateriales, Parque Tecnológico de San Sebastián, E-20009 San Sebastián, Spain

Quartz crystal microbalance (QCM or QCM-D) has become instrumental in life sciences and biosensor research. It is routinely and successfully used for monitoring interfacial processes, such as protein adsorption and conformational changes in the protein-adsorbed films, liposome–surface interactions and supported bilayer formation, and in the development of biosensor platforms. However, quantitative interpretation of QCM data from biological interfaces studied in liquid remains challenging. In vacuum, the so-called Sauerbrey relationship is routinely used to relate QCM frequency shifts due to the adsorbed layer to the mass of the adsorbed layer. Deviations from Sauerbrey relationship are typically observed when studying soft interfaces in liquids; these are interpreted in terms of layer viscoelastic properties. In this study, we develop and use a combined atomic force microscopy (AFM)–QCM setup to investigate the adsorption of protein ferritin on the surface of gold. First, we find that deviations from the Sauerbrey relationship in this system originate almost entirely from the heterogeneity of the protein films caused by the presence of impurities. Second, relying on the ability of AFM to visualize single ferritin molecules adsorbed on the surface, we find that the frequency shifts determined by QCM are not linearly related to the protein surface coverage.

The quartz crystal microbalance (QCM,^{1–3} or, more recently, QCM-D^{4,5}) has become instrumental in life sciences, soft interface, and biosensor research. It is used to monitor protein adsorption and conformational changes in the adsorbed protein films,^{6,7} to evaluate resistance of various coatings to protein adsorption,⁸ to

study liposome–surface interactions and supported bilayer formation,^{9–14} protein– and polymer–lipid interactions,^{8,15–20} and in the development of biosensors and biosensor platforms.^{21–27}

Despite the diverse applications of QCM mentioned above, quantitative interpretation of QCM data remains challenging, because of the large number of parameters that affect the measured response.^{3,28} A typical QCM experiment consists of monitoring changes in the resonance frequencies f_n and bandwidths Γ_n (related to dissipation D measured with the QCM-D^{4,5} as $D = 2\Gamma/f$; this parameter characterizes the amount of energy dissipated by the system) on several overtones n , e.g., as a film is allowed to form on the crystal surface. In the case of a thin, rigid, homogeneous film, these changes in the resonance frequencies between the (crystal + film) and the bare crystal are related to the areal mass density of the film via the Sauerbrey relationship:²⁹

$$\Delta F_n = -\frac{f_n}{\rho_q h_q} \rho_f h_f \quad (1)$$

- (9) Keller, C. A.; Kasemo, B. *Biophys. J.* **1998**, *75*, 1397.
- (10) Keller, C. A.; Glasmästar, K.; Zhdanov, V. P.; Kasemo, B. *Phys. Rev. Lett.* **2000**, *84*, 5443.
- (11) Reimhult, E.; Hook, F.; Kasemo, B. *Langmuir* **2003**, *19*, 1681.
- (12) Richter, R.; Mukhopadhyay, A.; Brisson, A. *Biophys. J.* **2003**, *85*, 3035.
- (13) Rossetti, F. F.; Bally, M.; Michel, R.; Textor, M.; Reviakine, I. *Langmuir* **2005**, *21*, 6443.
- (14) Reviakine, I.; Rossetti, F. F.; Morozov, A. N.; Textor, M. *J. Chem. Phys.* **2005**, *122*, 204711.
- (15) Rossetti, F. F.; Reviakine, I.; Csucs, G.; Assi, F.; Voros, J.; Textor, M. *Biophys. J.* **2004**, *87*, 1711.
- (16) Richter, R. P.; Maury, N.; Brisson, A. R. *Langmuir* **2005**, *21*, 299.
- (17) Richter, R. P.; Him, J. L. K.; Tessier, B.; Brisson, A. R. *Biophys. J.* **2005**, *89*, 3372.
- (18) Cho, N. J.; Kanazawa, K. K.; Glenn, J. S.; Frank, C. W. *Anal. Chem.* **2007**, *79*, 7027.
- (19) Cho, N. J.; Cho, S. J.; Cheong, K. H.; Glenn, J. S.; Frank, C. W. *J. Am. Chem. Soc.* **2007**, *129*, 10050.
- (20) Weng, K. C.; Kanter, J. L.; Robinson, W. H.; Frank, C. W. *Colloids Surf., B* **2006**, *50*, 76.
- (21) Graneli, A.; Rydstrom, J.; Kasemo, B.; Hook, F. *Biosens. Bioelectron.* **2004**, *20*, 498.
- (22) Svedhem, S.; Pfeiffer, I.; Larsson, C.; Wingren, C.; Borrebaeck, C.; Hook, F. *ChemBioChem* **2003**, *4*, 339.
- (23) Svedhem, S.; Dahlborg, D.; Ekeröth, J.; Kelly, J.; Hook, F.; Gold, J. *Langmuir* **2003**, *19*, 6730.
- (24) Larsson, C.; Rodahl, M.; Hook, F. *Anal. Chem.* **2003**, *75*, 5080.
- (25) Reuber, J.; Reinhardt, H.; Johannsmann, D. *Langmuir* **2006**, *22*, 3362.
- (26) Goubaidouline, I.; Vidrich, G.; Johannsmann, D. *Anal. Chem.* **2005**, *77*, 615.
- (27) Treput, S.; Mornet, S.; Benabdelhak, H.; Ducruix, A.; Brisson, A. R.; Lambert, O. *Langmuir* **2007**, *23*, 2647.
- (28) Hillman, A. R.; Jackson, A.; Martin, S. J. *Anal. Chem.* **2001**, *73*, 540.
- (29) Sauerbrey, G. Z. *Phys.* **1959**, *155*, 206.

* Corresponding author. E-mail: ireviakine@icbiomagune.es.

- (1) Cady, W. G. *Piezoelectricity*; McGraw-Hill Book Company, Inc.: New York, 1946.
- (2) Ward, M. D.; Buttry, D. A. *Science* **1990**, *249*, 1000.
- (3) Johannsmann, D. Studies of Viscoelasticity with the QCM. In *Piezoelectric Sensors*, 1st ed.; Steinem, C., Janshoff, A., Eds.; Springer: Berlin, Heidelberg, 2006; p 49.
- (4) Rodahl, M.; Hook, F.; Krozer, A.; Brzezinski, P.; Kasemo, B. *Rev. Sci. Instrum.* **1995**, *66*, 3924.
- (5) Rodahl, M.; Hook, F.; Kasemo, B. *Anal. Chem.* **1996**, *68*, 2219.
- (6) Hook, F.; Kasemo, B.; Nylander, T.; Fant, C.; Sott, K.; Elwing, H. *Anal. Chem.* **2001**, *73*, 5796.
- (7) Hemmersam, A. G.; Rechendorff, K.; Besenbacher, F.; Kasemo, B.; Sutherland, D. S. *J. Phys. Chem. C* **2008**, *112*, 4180.
- (8) Glasmästar, K.; Larsson, C.; Hook, F.; Kasemo, B. *J. Colloid Interface Sci.* **2002**, *246*, 40.

where f_n is the resonance frequency of the bare crystal, subscript f refers to the properties of the film, and Δf_n is the difference between the frequency of (crystal + film) and the bare crystal. The quantity $\Delta f/n$ is in this case independent of the overtone order n . Changes in the bandwidths are in this case negligibly small, because the film does not appreciably contribute to the energy dissipated by the crystal.

In practice, a non-negligible $\Delta\Gamma$ and a dependence of $\Delta f/n$ on n are observed experimentally when biomolecular films (e.g., of proteins adsorbed to the surface) are investigated with QCM. These have been interpreted in terms of layer viscoelastic properties,^{6,14,24,30–32} according to eq 2:³

$$\Delta\tilde{F}_n = \Delta F_n + i\Delta\Gamma_n = -\frac{f_n}{\rho_q h_q} h_f \rho_f \left(1 - \frac{\tilde{J}_f i 2\pi f_n \eta_{\text{liq}} \rho_{\text{liq}}}{\rho_f} \right) \quad (2)$$

where f and Γ are frequency and bandwidth, respectively, while h , ρ , η , and \tilde{J} are thickness, density, viscosity, and complex shear compliance of quartz (q), film (f), or liquid (liq). The Chalmers group uses a particular definition of the shear elastic moduli, based on the Voight–Kelvin model, in this equation.³³ The first term in brackets is the Sauerbrey mass (cf., eqs 1 and 2).

Essentially, this equation assumes that the acoustic response of an interface consists of a frequency-independent part (the Sauerbrey mass) and a frequency-dependent part, which is modeled as a viscoelastic response of the layer. Valid for homogeneous films, these assumptions become questionable in the case of heterogeneous films in liquids. Herein lay the difficulties in quantitative interpretation of QCM data: in the case of heterogeneous films in liquids, the frequency and bandwidth shifts contain a contribution from the surrounding liquid. This contribution has been frequently discussed, but studies that focus on investigating it are scarce. As a result, the meaning of the effective elastic constants obtained by fitting QCM data with eq 2 remains vague. Extracting quantitative information concerning size and surface coverage of individual adsorbed species (proteins, liposomes, micelles) remains a challenge and is the focus of several recent studies.^{34–38}

In this study, we report simultaneous in situ atomic force microscopy (AFM) and QCM measurements of ferritin adsorption onto gold with a new, robust design of the combined setup. Previous combinations of these techniques include those by Iwata

et al.,³⁹ who appear to have been the first to combine scanning probe microscopy and QCM, and several subsequent in situ^{40–44} and ex situ^{7,12,45} studies.

We find that the relationship between the number of adsorbed particles measured with the AFM and the frequency shift measured with QCM is not a linear one. We furthermore find that deviations from the Sauerbrey relationship are small for monolayers consisting predominantly of ferritin monomers, whereas they are significant in the case of nonpurified samples containing protein aggregates. However, we find that these deviations have a hydrodynamic, and not viscoelastic, origin.

THEORY

Equation 2 is obtained from the following more general expression by Taylor-expanding the tangent in powers of $k h_f$ and subtracting the contribution of liquid:

$$\Delta\tilde{F}_n = \frac{-Z_f(Z_f \tan(k h_f) - iZ_{\text{liq}})}{2\pi h_q \rho_q (Z_f + iZ_{\text{liq}} \tan(k h_f))} \quad (3)$$

where Z is the acoustic impedance $Z = (\rho/J)^{1/2}$, ρ is the density, and J the shear compliance; $k = \omega ZJ$ is the wave vector, and h is the thickness; subscripts q, f, and liq refer to quartz, film, and liquid, respectively; n is the overtone order. Frequencies, acoustic impedances, and compliances are understood to be complex quantities. Full numerical solutions of eq 3 are implemented in the modeling software (Q-Tools from Q-Sense and the public domain software QTM, available from <http://www.pc.tu-clausthal.de/de/forschung/ak-johannsmann/qcm-modellierung/>). It is convenient to discuss the ratio of bandwidth shift to the frequency shift, $(\Delta\Gamma)/(-\Delta f)$. Taking the ratio of real and complex parts of eq 3 and Taylor-expanding in $k h_f$, one obtains the following result for the ratio of bandwidth shift to frequency shift:

$$\frac{\Delta\Gamma}{-\Delta f} \approx \eta_{\text{liq}} 2\pi f_n \tilde{J}_f \quad (4)$$

where \tilde{J} is the elastic compliance of the film and η_{liq} is the viscosity of liquid.³

Somewhat neglected in the field of biological QCM is the hydrodynamics-based approach to interpreting QCM data. If the surface of the resonator is not smooth, the flow of the liquid in its vicinity deviates from planarity, affecting the frequency and bandwidth shifts.^{3,46–48} Therefore, following the approach of

- (30) Reimhult, E.; Larsson, C.; Kasemo, B.; Hook, F. *Anal. Chem.* **2004**, *76*, 7211.
 (31) Patel, A. R.; Frank, C. W. *Langmuir* **2006**, *22*, 7587.
 (32) Hook, F.; Voros, J.; Rodahl, M.; Kurrat, R.; Boni, P.; Ramsden, J. J.; Textor, M.; Spencer, N. D.; Tengvall, P.; Gold, J.; Kasemo, B. *Colloids Surf., B* **2002**, *24*, 155.
 (33) Voinova, M. V.; Rodahl, M.; Jonson, M.; Kasemo, B. *Phys. Scr.* **1999**, *59*, 391.
 (34) Macakova, L.; Blomberg, E.; Claesson, P. M. *Langmuir* **2007**, *23*, 12436.
 (35) Bingen, P.; Wang, G.; Steinmetz, N. F.; Rodahl, M.; Richter, R. P. *Anal. Chem.* [Online early access]. Doi: 10.1021/ac8011686. Published Online: Oct 1, 2008. <http://pubs.acs.org/cgi-bin/abstract.cgi/ancham/asap/abs/ac8011686.html>.
 (36) Tellechea, E.; Johannsmann, D.; Reviakine, I. *J. Phys. Chem. B*, submitted for publication, **2008**.
 (37) Johannsmann, D.; Reviakine, I.; Rojas, E.; Gallego, M. *Anal. Chem.*, in press, **2008**.
 (38) Tsortos, A.; Papadakis, G.; Mitsakakis, K.; Melzak, K. A.; Gizeli, E. *Biophys. J.* **2008**, *94*, 2706.

- (39) Iwata, F.; Kawaguchi, M.; Aoyama, H.; Fukaya, J.; Sasaki, A. *Thin Solid Films* **1997**, *299*, 78.
 (40) Kautek, W.; Dieluweit, S.; Sahre, M. *J. Phys. Chem. B* **1997**, *101*, 2709.
 (41) Borovsky, B.; Mason, B. L.; Krim, J. *J. Appl. Phys.* **2000**, *88*, 4017.
 (42) Choi, K. H.; Friedt, J. M.; Frederix, F.; Campitelli, A.; Borghs, G. *Appl. Phys. Lett.* **2002**, *81*, 1335.
 (43) Bund, A.; Schneider, O.; Dehnke, V. *Phys. Chem. Chem. Phys.* **2002**, *4*, 3552.
 (44) Heim, L. O.; Johannsmann, D. *Rev. Sci. Instrum.* **2007**, *78*, 013902.
 (45) Dimitrievski, K.; Zach, M.; Zhdanov, V. P.; Kasemo, B. *Colloids Surf., B* **2006**, *47*, 115.
 (46) Martin, S. J.; Frye, G. C.; Ricco, A. J.; Senturia, S. D. *Anal. Chem.* **1993**, *65*, 2910.
 (47) Urbakh, M.; Tsionsky, V.; Gileadi, E.; Daikhin, L. Probing the solid/liquid interface with quartz crystal microbalance. In *Piezoelectric Sensors*, 1st ed.; Steinem, C., Janshoff, A., Eds.; Springer: Berlin, Heidelberg, 2006; p 111.
 (48) Urbakh, M.; Daikhin, L. *Phys. Rev. B* **1994**, *49*, 4866.

Urbakh and Daikhin,^{3,47,48} the complex frequency shift caused by a shallow roughness can be written as

$$\Delta\tilde{f} \approx \frac{1}{2\pi\rho_q h_q} \sqrt{\frac{\rho_{\text{liq}}\omega\eta_{\text{liq}}}{2}} \left[\left(1 + 2\frac{h_r^2}{\delta^2} \right) - i \left(1 + 3\sqrt{\pi}\frac{h_r}{l_r\delta} - 2\frac{h_r^2}{\delta^2} \right) \right] \quad (5)$$

where $h_r \ll l_r$ are rms roughness and the lateral roughness scale, of Gaussian roughness, respectively, and $\delta = [\eta_{\text{liq}}/(\rho_{\text{liq}}\pi f n)]^{1/2}$ is the penetration depth of the acoustic waves in liquid. In the limit of a smooth crystal ($h_r \rightarrow 0$), this equation reduces to the Kanzawa–Gordon relationship for a crystal in a Newtonian liquid.⁴⁹ The $(\Delta\Gamma)/(-\Delta F)$ ratio can also be obtained from eq 5:

$$\frac{\Delta\Gamma}{-\Delta F} = \frac{\frac{1}{2\pi\rho_q h_q} \left(n \frac{\rho_{\text{liq}} h_r^2}{\rho_q h_q \delta} \right)}{\frac{1}{2\pi\rho_q h_q} \left(\frac{3\sqrt{\pi}\rho_{\text{liq}} h_r^2}{2 l_r} \right)} = \frac{2}{3\sqrt{\pi}} \frac{l_r}{\delta} = l_r \sqrt{n} \left(\frac{2\sqrt{\rho_{\text{liq}} f}}{3\sqrt{\eta_{\text{liq}}}} \right) \quad (6)$$

(the term h_r^2/δ^2 was neglected in the above step). It has to be kept in mind that a net change in the crystal thickness (Sauerbrey mass) is not accounted for in this approach—only differences in the frequency and bandwidth relative to a smooth crystal due to changes in roughness.

MATERIALS AND METHODS

Materials. Chemicals used in preparing buffers (HEPES, sodium chloride, sodium hydroxide, sodium acetate, acetic acid), HCl, and horse spleen ferritin, were purchased from Sigma-Aldrich (Madrid, Spain). Ammonium hydroxide and hydrogen peroxide were purchased from Scharlab (Barcelona, Spain). The 5 MHz quartz crystals with evaporated gold electrodes were purchased from Q-Sense (Gothenburg, Sweden).

Protein Purification. For purification by size exclusion chromatography, the stock solution of ferritin was dissolved in 10 mM HEPES pH 7.4 buffer containing 60 mM NaCl and centrifuged at 10 000g for 10 min at room temperature to remove large aggregates. The supernatant was injected onto a Superose 6 10/300 size exclusion column, mounted on an AKTA Purifier 10 system (GE Healthcare, Sweden), pre-equilibrated with at least two column volumes of the same buffer. The separation was performed at a flow rate of 0.5 mL/min and monitored by measuring conductivity and UV absorbance at 190 and 280 nm. Fractions were collected with a Frac 950 fraction collector. Sample absorbance was measured at 280 nm and converted to concentration using a previously determined molar extinction coefficient of 4 mL mg⁻¹ cm⁻¹. We note that the absolute protein concentrations are not relevant to the results of our study. Fractions were analyzed by dynamic light scattering using a NanoSizer (Malvern, U.K.) and electron microscopy (on a JEOL JEM-2100F transmission electron microscope). In some experiments, the monomer fraction was purified twice. Fresh monomer fraction (not more than 2 days old), and the nonpurified starting solution, were used in the AFM–QCM experiments. They are referred to as the “purified” and “nonpurified” preparations, respectively.

(49) Kanazawa, K. K.; Gordon, J. G. *Anal. Chem.* **1985**, *57*, 1770.

Surface Preparation. Quartz crystals with evaporated gold electrodes used as substrates in this work were cleaned overnight in 2% sodium dodecyl sulfate (SDS) solution, rinsed with nanopure water, cleaned in a mixture of ammonium hydroxide and hydrogen peroxide (1:1:1.5 with water) at 80 °C for 10 min, rinsed once more with nanopure water, and cleaned in air plasma for 12 min in a PDC-002 plasma cleaner set at “high” (30 W). After cleaning, the crystals were used immediately. After each experiment, the crystals were cleaned in 2% SDS overnight and rinsed with copious amounts of water. We found it was quite critical for the success of the experiments not to let the protein dry on the surface.

Combined Quartz Crystal Microbalance–Atomic Force Microscopy Setup. For the combined AFM–QCM experiments, quartz crystals were mounted on the sample stage of the Veeco Multimode atomic force microscope connected to a Nanoscope V controller, equipped with the variable temperature accessory (MMHC35-100, Veeco, Instruments, Santa Barbara, CA). This accessory contains a “J” (125 μm) scanner that has a socket for mounting the Peltier element for controlling sample temperature and a cable terminating with a 7-pin Lemo plug for connecting the Peltier element and the thermocouple to the temperature controller. A holder for the QCM crystals containing two leads that fit into the socket on top this scanner was designed. The cable used in the variable temperature accessory to connect the Peltier element and the thermocouple to the temperature controller was used to connect the leads in the holder to the SA250C network analyzer (Saunders, AZ) installed in a personal computer via a pi-network fixture (Saunders, AZ) using a matching 7-pin, 12 mm Lemo socket (RS Components BV, Germany). The network analyzer was controlled by the software package QTZ (Resonant Probes GmbH, Goslar, Germany). Quartz crystal was fixed to the electrodes of the holder with colloidal silver (Mono-comp Instrumentación S.A., Madrid, Spain) to ensure proper electrical connections. Grounding the front electrode of the quartz crystal via a BalUn transformer (ADT1 from Mini-circuits, Brooklyn, NY) did not affect the measurements. All the measurements reported in this manuscript were therefore performed without the transformer.

In the beginning of each experiment, a freshly cleaned QCM crystal was mounted on the holder on top of the scanner and the tapping mode fluid cell with an S-shaped silicon O-ring (Veeco) was assembled on top. The cell was filled with buffer containing 10 mM HEPES, pH 7.4, and 150 mM NaCl solution. The tip was brought in close proximity of the surface of the crystal. At that point, resonance frequencies and bandwidth on the overtones from $n = 3$ to $n = 15$ were found, and their evolution was monitored as a function of time. [In some measurements, it was possible to collect data on overtones $n = 17$ and $n = 19$ as well (not shown).] The system (both AFM and QCM) was allowed to equilibrate for approximately 30–40 min (until the QCM signals became stable), at which point images of the bare gold surface were collected. Image collection did not interfere with QCM operation.

Once it was established that the gold surface was free of impurities, the AFM tip was withdrawn from the surface, 0.3–0.5 mL of the protein solution in appropriate buffer (see below) was passed through the (~50 μL) fluid cell of the AFM, and the QCM signals (ΔF and $\Delta\Gamma$) were allowed to reach stable values.

To vary surface coverage of ferritin, protein concentration and salt concentration were varied between 30 and 100 $\mu\text{g}/\text{mL}$ and 60 and 150 mM NaCl, respectively. Adsorption of ferritin is sensitive to ionic strength.^{50,51} The combination of these two parameters, therefore, allowed a wide range of surface coverages to be reliably achieved. Imaging was always performed at 150 mM NaCl. Therefore, the samples were rinsed with the 150 mM NaCl containing buffer prior to imaging.

The injection–stabilization–rinsing–imaging process was typically repeated several times in the course of one experiment. This allowed the images of protein at different surface coverage to be related to the frequency and bandwidth shifts observed by QCM.

The presence of bubbles was found to severely affect the QCM signals, predominantly at lower overtones. For this reason, the 15 MHz overtone ($n = 3$) had to be excluded from analysis in most of the experiments.

AFM images were exported in JPEG format and analyzed in Adobe Photoshop to extract particle counts per unit area.

RESULTS

Protein Purification. Commercial ferritin samples contain various impurities: aggregates, dimers, and products of protein decomposition.^{52,53} Size exclusion chromatography was used to isolate the predominantly monomer-containing fraction (Figure 1a), whereas dynamic light scattering and transmission electron microscopy (TEM) (Figure 1b–e) were used to characterize the starting solution and the various fractions that emerged from the column.

After several trials, a set of conditions was found which gave best (though imperfect) separation of the predominantly monomer-containing fraction (Figure 1a). On average, species contained in this fraction exhibited a size of ~ 14 nm (Figure 1b) and appeared isolated on the TEM images (Figure 1d). On the contrary, the solutions of nonpurified ferritin typically contained clusters of molecules (Figure 1e) and exhibited broad size distributions (Figure 1c).

Both the monomer fraction (eluting at ~ 14 mL) and the aggregates fraction (eluting at ~ 9 mL) migrated as single species accompanied by only minor contamination upon subsequent purification (not shown). Therefore, in some of the AFM–QCM experiments, such twice-purified monomer fractions were used.

Adsorption of Purified and Nonpurified Ferritin on Gold: The Quartz Crystal Microbalance–Atomic Force Microscopy Combination. The operation of the combined AFM–QCM instrument (Figure 2) is not so different from that of the individual ones and is described in detail in the Materials and Methods. QCM results from the AFM–QCM combined setup are shown in Figure 3. Typical curves—a decrease of the $\Delta F/n$ as a function of time after injection—were observed for both nonpurified and purified proteins (Figure 3, parts a and b). The asymptotic frequency shifts depended on the ferritin concentration and, for the purified protein, on the ionic strength. As expected, higher

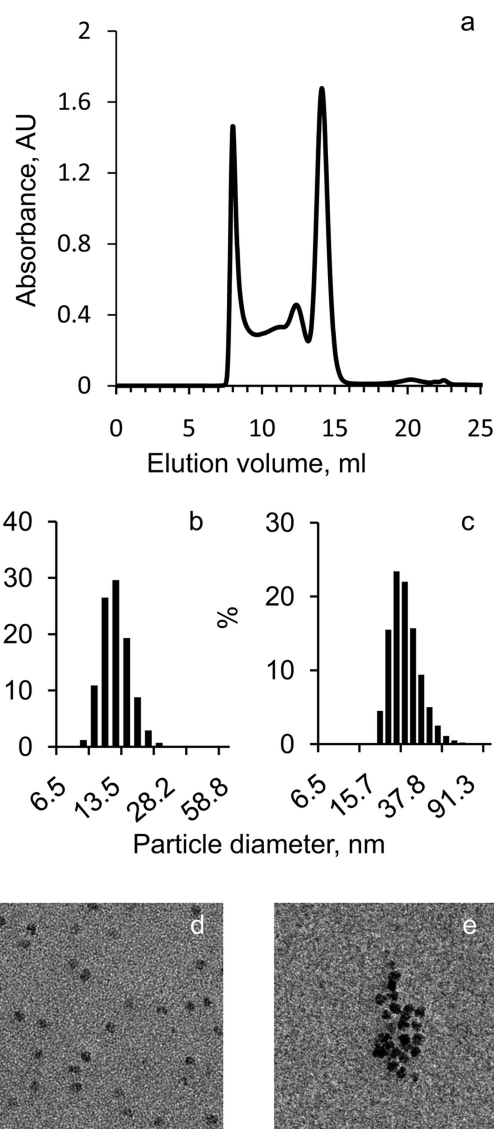


Figure 1. Ferritin purification. (a) Commercial ferritin used in this study was purified by size exclusion chromatography. A typical chromatogram is shown. The peak at ~ 14 mL corresponds to ferritin monomers, and the smaller peak at ~ 12.5 mL corresponds to dimers. Smaller peaks appearing around 20 mL correspond to protein subunits. Each of the peaks appearing at ~ 9 and ~ 14 mL eluted as single species, with only minor contaminants, upon subsequent injections (not shown). (b) Dynamic light scattering analysis of the monomer fraction. Number-averaged distribution is shown (mean size ~ 14 nm). It is clear that some small amount of dimers or higher-order aggregates are still present in this fraction. This is confirmed by comparing the intensity-averaged distribution (mean size ~ 16 nm, not shown) with the number-averaged one. The corresponding electron microscopy image of this fraction is shown in (d), where individual iron particles of ~ 6 nm can be seen. (c) Dynamic light scattering analysis of the nonpurified ferritin. The corresponding electron microscopy image of this preparation is shown in (e), where clusters of ~ 6 nm iron particles separated by ~ 13 nm can be seen. The images in (d) and (e) are $156 \times 156 \text{ nm}^2$. Unstained preparations were used for the TEM analysis. Therefore, only the core iron particles are visible. Center-to-center distances between the iron particles in the clusters shown in (e) correspond to the protein diameter (~ 13 nm).

protein concentrations resulted in frequency shifts of greater magnitude (more negative), as did higher ionic strengths, consistent with the previous reports of electrostatic repulsion

(50) Hook, F.; Rodahl, M.; Brzezinski, P.; Kasemo, B. *J. Colloid Interface Sci.* **1998**, *208*, 63.

(51) Johnson, C. A.; Yuan, Y.; Lenhoff, A. M. *J. Colloid Interface Sci.* **2000**, *223*, 261.

(52) Thomas, B. R.; Carter, D.; Rosenberger, F. *J. Cryst. Growth* **1998**, *187*, 499.

(53) Petsev, D. N.; Thomas, B. R.; Yau, S. T.; Vekilov, P. G. *Biophys. J.* **2000**, *78*, 2060.

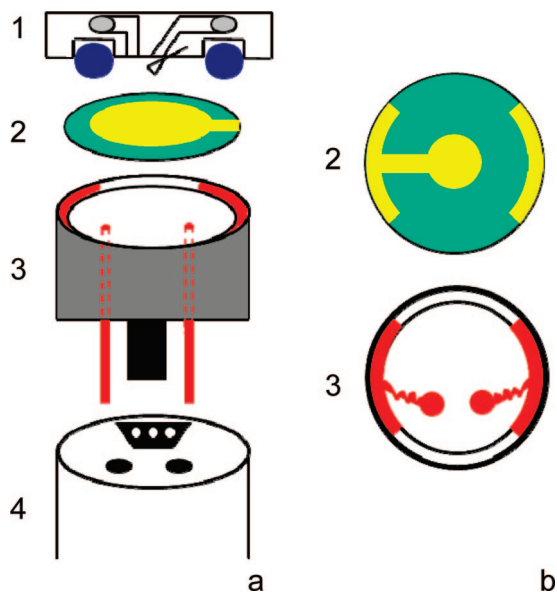


Figure 2. AFM–QCM combination. (a) Side view of the QCM–AFM combination design based on the scanner included with the variable temperature accessory sold by Veeco for the MultiMode AFM. (1) Fluid cell of the MultiMode AFM (the head of the microscope is not shown). In this figure, the fluid cell is shown together with the O-ring (blue), but the arrangement works as well in the absence of the O-ring. (2) A 14 mm 5 MHz quartz crystal (green) with key-hole-shaped gold electrodes. Only the top electrode is shown in this case. (3) Holder used to mount the crystal on top of the scanner. (4) The top of the scanner that comes with the variable temperature accessory contains a five-pole socket (three poles at the top (white circles) and two poles at the bottom (black circles)) for the Peltier–thermocouple assembly. The bottom of the holder (3) is machined to fit exactly into the socket on top of the scanner (4). It contains the two leads for connecting the crystal to the impedance analyzer. These leads are soldered to the copper electrodes that line the sides of the holder (shown in red in (b)). The drawing is not to scale. (b) Bottom view of the quartz crystal (2) and the top view of the holder (3) with the electrode arrangement. The electrodes in the holder are shown in red.

between the adsorbing ferritin molecules at neutral pH.⁵⁰ In the case of purified protein, frequency shifts of up to -86 Hz were observed (averaged over overtones with $n = 5$ to $n = 13$). This corresponds to a Sauerbrey mass of ~ 1540 ng/cm². In the case of nonpurified protein, experiments with high enough protein concentration were not conducted in the AFM–QCM cell for the reasons described below. Instead, experiments were performed in a closed stagnation-point flow cell (not mounted on the AFM, not shown). The frequency shifts observed with this closed, stagnation-point flow QCM cell, in the range of protein concentrations where frequency shifts no longer depended on the protein concentration, were $\sim -95 \pm 8$ Hz (averaged over overtones with $n = 5$ to $n = 13$, 10 independent experiments). The values reported for adsorption of ferritin on gold by other authors are of the order of -250 Hz for a 9 MHz crystal,⁵⁴ which would translate into ~ -77 Hz for the 5 MHz one, and ~ -70 Hz reported by Höök et al.⁵⁰ for a monolayer of ferritin on hydrophobically modified gold-coated 5 MHz QCM crystal at a salt concentration similar to ours. Hemmersam et al.⁷ reports maximum frequency shifts of ~ -86 Hz.

Interestingly, in the case of nonpurified protein, an increase in the $\Delta\Gamma$ as a function of time after injection and a corresponding dependence of the frequency shift $\Delta F/n$ on the overtone order n —signifying non-Sauerbrey behavior—were also observed (Figure 3a). On the other hand, in the case of purified protein, the change in the bandwidth $\Delta\Gamma$ and the dependence of the frequency shift $\Delta F/n$ on the overtone order n were either negligible or significantly smaller than observed with the nonpurified protein (Figure 3b). This is more clearly illustrated in Figure 3c–e. In Figure 3c, the value of the frequency shift $\Delta F/n$ at a particular overtone divided by the value of $\Delta F/n$ averaged over overtones $n = 3$ to $n = 13$ is plotted as a function of the overtone order n . There is a clear dependence of $(\Delta F/n)/\langle\Delta F/n\rangle$ on the overtone order n in the case of the nonpurified protein (blue rhombi), whereas the dependence is much weaker in the case of purified protein (red squares). Similar results were obtained in the closed stagnation-point flow cell (not mounted on the AFM): $(\Delta F/n)/\langle\Delta F/n\rangle$ was also linear in the overtone order n , with a negative slope (not shown).

The $\Delta\Gamma/\Delta F$ ratio is nearly zero for the purified protein but depends on the overtone order in the case of the nonpurified one (Figure 3d). Note that the plot of the $\Delta\Gamma/\Delta F$ ratio versus the overtone order is not a straight line. The value of the ratio levels off at higher frequencies. This leveling off cannot be attributed to crystal or contact problems (higher-order overtones are notoriously more sensitive to the presence of the anharmonic sidebands and contact problems), because all of these would lead to a larger bandwidth shift, not a smaller one.

Values presented in Figure 3, parts c and d, are obtained by averaging data from experiments with very different frequency shifts. To examine, whether the shift in bandwidth was correlated with the magnitude of the frequency shift, the values of $\Delta\Gamma$ were plotted versus those of ΔF (the so-called DF plot;¹⁰ Figure 3e). Indeed, it can be seen that more complete layers (ones characterized by a larger $-\Delta F$) dissipate more energy (exhibit a greater $\Delta\Gamma$ shift). In the case of purified protein, the bandwidth shifts are negligible up to a frequency shift of ~ -50 to -60 Hz. In the case of the nonpurified protein, non-negligible bandwidth shifts are observed at smaller frequency shifts.

In summary, deviations from Sauerbrey behavior were observed with both purified and nonpurified preparations, but in the latter case, they were more significant and were observed at smaller values of the frequency shift than in the former case. The frequency dependence of the bandwidth shift to frequency shift ratio, $(\Delta\Gamma)/(-\Delta F)$, can be used to evaluate whether these deviations from the Sauerbrey behavior are of viscoelastic or hydrodynamic origin. According to eq 6, hydrodynamic effects should lead to a square-root frequency dependence of the ratio. Indeed, the plot of $(\Delta\Gamma)/(-\Delta F)$ versus \sqrt{n} is a straight line (Figure 4). Its slope yields a lateral roughness scale l_r of ~ 23 nm for the nonpurified protein. Interestingly, this is consistent with the size of ferritin dimers, a major impurity in the nonpurified preparations (Figure 1), although this may be a coincidence. In any case, according to eq 4, the bandwidth shift to frequency shift ratio should be linear in n , and not in $n^{1/2}$. Therefore, deviations from the Sauerbrey behavior observed in the case of nonpurified ferritin adsorption on gold arise from hydrodynamic effects.

(54) Caruso, F.; Furlong, D. N.; Kingshott, P. J. *Colloid Interface Sci.* **1997**, *186*, 129.

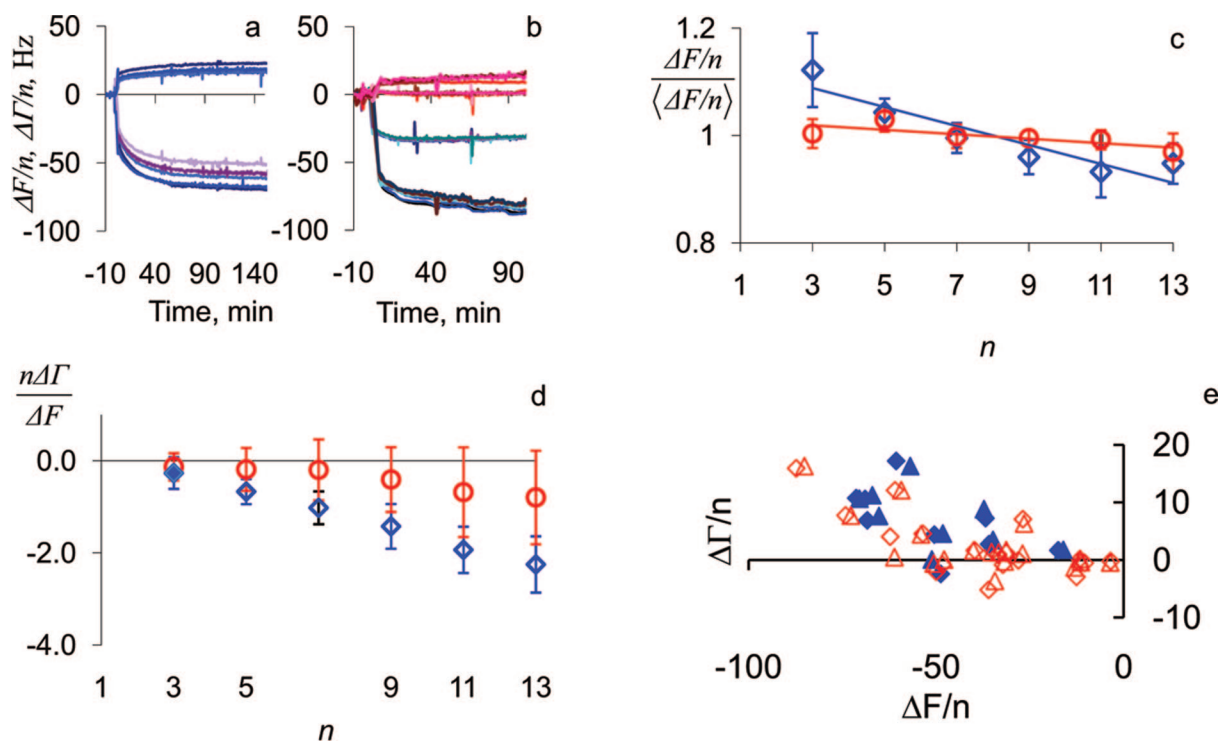


Figure 3. Adsorption of nonpurified and purified ferritin on gold: QCM data. (a) A typical QCM response observed in the AFM–QCM setup with nonpurified protein. The frequency is observed to decrease while bandwidth is observed to increase as the protein adsorbs to the surface of the crystal. Overtones $n = 5$ to $n = 13$ are shown. (b) Typical QCM curves observed in the AFM–QCM setup with purified protein. Results of two separate experiments are shown. In both cases, the frequency is observed to decrease. No change in the bandwidth is detected in one experiment, while some change in bandwidth is observed in the experiment with the larger frequency shift. Overtones $n = 3$ to $n = 13$ are shown. (c) The dependence of the QCM response on frequency in the case of the nonpurified protein (blue rhombi), and of the purified protein (red circles), is illustrated in this figure by plotting the ratio between the value of the frequency shift at a particular overtone, scaled by the overtone order, and the frequency shift, scaled by the overtone order, averaged over the overtones (spread over the mean). In this way, data from experiments with different average frequency shifts (caused by injecting different amounts of protein) could be combined on one plot. In the case of nonpurified protein, there is a linear relationship between the $(\Delta F/n)/\langle \Delta F/n \rangle$ ratio and the overtone order, with a slope of -0.018 and an intercept of 1.14 . Experiments performed with a closed stagnation-point flow QCM chamber (not shown) yielded a similar linear relationship, with the slope of -0.013 and an intercept of 1.05 . The difference between these two sets of values is not statistically significant. In the case of purified protein, the $(\Delta F/n)/\langle \Delta F/n \rangle$ ratio is almost independent of the overtone order. (d) A further illustration of the differences in QCM response from the purified (red circles) and the nonpurified (blue rhombi) protein preparations is apparent when the $\Delta\Gamma/\Delta F$ ratio is examined. It is nonlinear in frequency in the case of the nonpurified protein but is ~ 0 in the case of the purified protein. (e) To examine the dependence of the bandwidth shift on the magnitude of the frequency shift, the $\Delta\Gamma$ is plotted as a function of ΔF for purified (red open symbols) and nonpurified (blue filled symbols) ferritin, for overtones $n = 7$ (rhombi) and $n = 9$ (triangles). At small frequency shifts (little protein on the surface), the bandwidth shifts are negligible but begin to rise as the magnitude of the frequency shift decreases. It rises faster in the case of the nonpurified protein than in the case of the purified one.

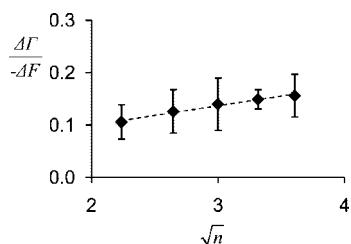


Figure 4. Plot of the ratio of the bandwidth shift to the frequency shift vs $n^{1/2}$. The ratio of bandwidth shift to frequency shift, $(\Delta\Gamma)/(-\Delta F)$, is plotted as a function of the square root of the overtone order, n , for $n = 5$ – 13 . The plot is clearly a straight line. The slope of this line yields the lateral roughness scale, l_r , of ~ 23 nm according to eq 6. Error bars are standard deviations, from an average of eight experiments.

Similar analysis did not yield a definitive answer in the case of purified protein. Values ranging from ~ 3 to 19 nm were obtained from similar plots (not shown), but in at least two experiments the slope of the plot, similar to the one shown in

Figure 4, was negative, and in most experiments, the values of the bandwidth shifts were simply too small to be reliable.

The AFM–QCM combination employed in this study affords an opportunity to directly examine the interface investigated by QCM (Figure 5). Prior to protein injection, QCM crystals appear clean and homogeneous (Figure 5a). A protein layer becomes visible after injection and equilibration (Figure 5b–f). The images of the nonpurified ferritin preparation (Figure 5, parts b and c) are in fact quite similar to those previously published by Johnson et al.⁵¹ and Hemmersam et al.⁷

The most striking difference between the nonpurified (Figure 5, parts b and c) and purified (Figure 5d–f) protein preparations is the heterogeneity of the former. The aggregates that are observed in the nonpurified ferritin preparation originate from solution. Their presence is consistent with the analysis of the ferritin stock solutions before purification (Figure 1).

Despite the roughness typically associated with the evaporated gold surface (Figure 5, parts a and f), and the presence of the aggregates in the case of nonpurified protein preparations (Figure

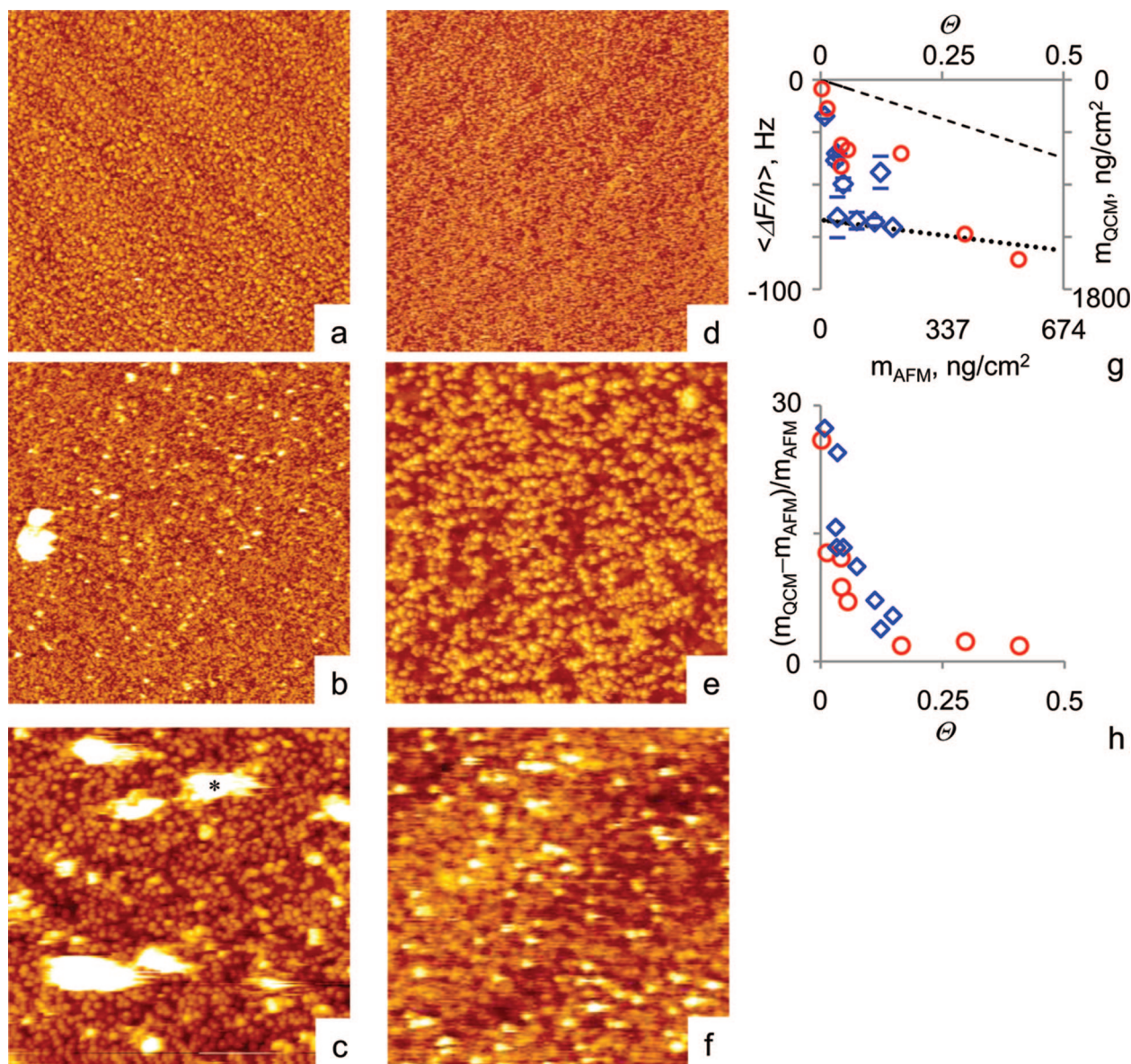


Figure 5. Adsorption of nonpurified and purified ferritin on gold: AFM and combined results. (a) A tapping mode image of the bare gold electrode on a QCM crystal, imaged in buffer prior to ferritin adsorption. Grains, between 50 and 150 nm in size, are visible. Diagonal waviness, apparent in the image, is typical of surfaces prepared by physical vapor deposition. The image is $5 \times 5 \mu\text{m}^2$. Z-scale: 25 nm. (b and c) Tapping mode images of nonpurified ferritin adsorbed on the freshly cleaned gold electrodes of the QCM crystals, obtained in liquid. The images are $5 \times 5 \mu\text{m}^2$ (50 nm) and $1 \times 1 \mu\text{m}^2$ (50 nm), respectively. Aggregates (white objects, one of which is indicated with an asterisk) as well as individual ferritin molecules (brown balls) are clearly visible. (d–f) Tapping mode images of purified ferritin adsorbed on the QCM crystals, obtained in liquid. The images are $10 \times 10 \mu\text{m}^2$ (50 nm), $2 \times 2 \mu\text{m}^2$ (50 nm), and $2 \times 2 \mu\text{m}^2$ (15 nm), respectively. Individual ferritin molecules are visible in (e) and (f), while (d) is presented underscore how homogeneous the surface typically is when purified ferritin is used in the experiments. Outlines of the gold grains are visible in (e) and (f). Images from different experiments are shown. (g) Frequency shifts, $\Delta F/n$, observed by QCM are plotted vs surface coverage, Θ , derived from the particle counts obtained from AFM images. For convenience, the frequency shifts were converted into the areal mass density using the Sauerbrey relationship, whereas the surface coverage was converted into the areal mass density assuming that the molecular weight of ferritin is ~ 990 kDa. Red circles: purified protein. Blue rhombi: commercial ferritin preparations. For each measurement, the $\Delta F/n$ values on overtones $n = 3$ or $n = 5$ to $n = 13$ were averaged, and the averaged value is what is plotted here. Each point corresponds to one experiment. Error bars (standard deviations) indicate the spread between the overtones. In the case of data points without the error bars, the size of the error bars was smaller than the size of the rhomb used to represent the data. Aggregates can be taken into account only approximately when counting individual ferritin molecules in AFM images; therefore, no quantitative conclusions could be drawn from the data obtained with the nonpurified protein. For this reason, experiments leading to higher particle counts with nonpurified protein were not attempted. The black dashed and dotted lines represent the dry Sauerbrey mass and the “hydrated” mass of the water + ferritin layer, respectively. In the calculation of the latter, the layer was represented as a 12 nm thick slab composed of ferritin molecules and water. Packing density of ferritin determined by AFM was used to calculate the protein and water volume fractions in the layer, and ferritin molecular weight was taken as 990 kDa. (h) Evolution of the difference between QCM-derived and AFM-derived mass, scaled by the AFM-derived mass, is plotted as a function of surface coverage for purified (red circles) and nonpurified (blue rhombi) ferritin preparations.

5c), it was possible to visualize and count individual ferritin molecules at various packing densities (Figure 5, parts c, e, and f). Spherical particles of ferritin are easily identifiable in Figure 5, parts c and e; their appearance is quite distinct than that of the underlying gold grains visible in Figure 5f.

Interpretation of these images presents a number of challenges. First among those is the tip convolution. It is a well-established that the size of individual particles measured by AFM depends on their packing density due to tip convolution effects. Sparsely packed particles will appear larger than densely packed particles of the same size. It is also well-established, however, that center-to-center distances between particles, and particle counts, obtained from AFM images are not affected by this artifact.⁵⁵ However, tip convolution does prevent ferritin monomers and dimers from being reliably distinguished from each other at low packing densities. In the case of purified ferritin preparations, we can be certain that protein at the surface is monomeric: there are almost no dimers present in solution (Figure 1); the surface-adsorbed protein does not diffuse and can therefore not dimerize. Supporting this assertion, correct sizes (~11–14 nm) for ferritin monomers were obtained from images where the packing density was sufficiently high (not shown). On the other hand, in the case of nonpurified preparations, we cannot always be certain that particles adsorbed to the surface are ferritin monomers. The possible presence of surface-adsorbed dimers represents the second, more subtle, difference between the purified and nonpurified ferritin preparations. Due to these two problems, particle counts obtained from the AFM images of the nonpurified preparation could only be considered estimates.

In Figure 5g, the frequency shifts, averaged over overtones with $n = 5$ to $n = 13$, are plotted as a function of ferritin packing density determined from the AFM images. The most striking feature of this plot is its nonlinearity, apparent in both cases (purified and nonpurified protein). In the case of purified protein, approximately 50% of the maximum frequency shift is observed by the time the packing density reaches 0.1, and the other 50% is attained while surface coverage changes from 0.1 to 0.4. The highest packing density reached in our experiments with the purified preparations is ~0.4, compared with the expected 0.55 for the RSA adsorption isotherm⁵⁶ and 0.5 reported by Lavalley et al.⁵⁵ for apoferritin on mica. The nonlinearity is more apparent in the case of the nonpurified protein, where ~70% of the maximum frequency shift is reached by the time the packing density reaches ~0.1.

It is interesting to examine, how the difference in the mass of the adsorbed layer evaluated with the two techniques changes with the surface coverage. The difference between the QCM-derived mass, calculated according to the Sauerbrey relationship, and the AFM-derived mass, scaled by the AFM-derived mass, is plotted versus the surface coverage in Figure 5h. This quantity corresponds to the extent to which QCM overestimates the mass of the adsorbed protein layer. It decreases with increasing surface coverage, reaching values of ~1.8 at the coverage of ~0.4 in the case of the purified protein preparation. If this quantity is interpreted in terms of the solvent (water) trapped between the adsorbed particles, the expected value can be calculated as follows:

$$\frac{m_{\text{QCM}} - m_{\text{AFM}}}{m_{\text{AFM}}} = \frac{m_{\text{solvent}}}{m_{\text{ferr}}} = \frac{(2\pi R^3/\Theta - 3\pi R^3)\rho_{\text{solvent}}}{4/3\pi R^3\rho_{\text{ferr}}} = \left(\frac{3}{2\Theta} - 1\right)\frac{\rho_{\text{solvent}}}{\rho_{\text{ferr}}} \quad (7)$$

where R is the radius of the ferritin molecule, ρ is the density of the solvent and the ferritin, respectively, and Θ is the surface coverage. For a collection of randomly close-packed spheres ($\Theta = 0.55$) of the same density as the solvent, a value of ~1.73 is expected. Similar values have recently been reported for surface-adsorbed spherical micelles.³⁴ Accounting for the higher density of ferritin (~1.6 g/cm³), a value of ~1.7 is expected at a packing density of 0.4. This agrees with the observations surprisingly well.

We would like to note that inherent in this interpretation is an assumption that QCM response can be related to the adsorbed particle mass even at the early stages of the adsorption process, when hydrodynamic contributions to the frequency shift may dominate over the gravimetric one. This regime requires further investigation.

DISCUSSION

Purification of biological entities is an involved subject. Protein preparations destined for crystallization trials, which could arguably be considered more pure than most, typically still contain percentage amounts of impurities. In this study, the effect of such impurities present in the adsorbing protein solution on the QCM response is described. In our case, these impurities are ferritin aggregates of various orders (dimers, trimers, and so on, Figures 1 and 5). These are by definition entities with close protein–protein contacts.

Interpretation of QCM response (frequency and bandwidth shift) in terms of a model that describes homogeneous viscoelastic films (eq 2) implies contributions from (visco)elastic properties of the proteins themselves and from the interactions between them. Having indeed observed in the case of aggregate-containing ferritin preparations bandwidth shifts and dependence of the frequency shift on the overtone order (Figure 3)—effects apparently consistent with the predictions of eq 2—we find instead that these effects are of hydrodynamic origin (Figure 4).

Furthermore, by directly comparing frequency shifts with the surface coverage derived from the AFM images (Figure 5) we observe experimentally that the relationship between the two is not a linear one, even in the case of the pure protein preparation.

The rapid saturation of the frequency shift observed in the case of the nonpurified protein is a combination of two effects: adsorption of aggregates themselves, on one hand, and the poor sensitivity of the QCM to adsorption of material in spaces between the aggregates due to the presence there of the trapped solvent. This mechanism must surely operate, and be responsible for, the nonlinearity that is observed in the case of the purified protein. However, the experiments with the purified protein, although far more reliable, were not amenable to simple analysis in terms of analytical models, such as that exemplified by eq 6. In a separate study, finite element calculations based on the incompressible Navier–Stokes equation modeling QCM experiment are shown to reproduce experimental data obtained with the purified protein; the deviations from Sauerbrey behavior and the nonlinearity in

(55) Lavalley, P.; Gergely, C.; Lustig, A.; Ball, V. J. *Chem. Phys.* **2000**, *113*, 8212.

(56) Hinrichsen, E. L.; Feder, J.; Jossang, T. *Phys. Rev. A* **1990**, *41*, 4199.

the dependence of the frequency shift versus surface packing density are shown to be of hydrodynamic origin.³⁷

At this point, it is relevant to mention the recent study of ferritin adsorption at surfaces of various materials by a combination of QCM and ex situ AFM performed in air.⁷ In Figure 4 of their manuscript, Hemmersam et al. demonstrate what they call a remarkable overlap between AFM and QCM data. It is interesting to note, however, the ranges of the Δf and particle density axes of their figure: the former spans from 0 to -86 Hz, whereas the latter merely reaches 1000 particles per square micrometer, or surface coverage of 0.12. Their data, in fact, are entirely consistent with ours: in the case of the nonpurified protein, the shift in frequency nearly saturates by the time the coverage reaches ~ 0.1 (blue rhombi in Figure 5g). We would like to further remark that AFM allows imaging proteins in liquids, as was done in our study.

CONCLUSIONS

In this study, we investigate the effect of impurities typically present in biochemical preparations on the response of QCM to the formation of a surface-adsorbed film. We demonstrate that deviations from the Sauerbrey relationship typically attributed to

the viscoelastic properties of the films actually originate from hydrodynamic effects. We furthermore demonstrate that the relationship between the frequency shift and protein surface coverage is not a linear one.

ACKNOWLEDGMENT

The authors thank Uwe Cronjager (TU Clausthal) for making the AFM-mountable holder for QCM crystals, Joseba Irigoyen and Marco Moller (CIC biomaGUNE) for expert assistance with the atomic force and transmission electron microscopy, respectively, and Edurne Tellechea (CIC biomaGUNE) and Dr. Alexander N. Morozov (University of Edinburgh) for discussions and suggestions. I.R. is greatly indebted to Professor Diethelm Johannsmann for many discussions and the derivation of eq 6 and thanks the Alexander von Humboldt Foundation for awarding him a Research Fellowship; he also thanks the Department of Industry of the Basque Country for the generous start-up funding.

Received for review June 23, 2008. Accepted September 15, 2008.

AC8012829